

Charged heavy vector boson production at the Large Hadron Collider

Dal Soo Oh and M. H. Reno

Department of Physics and Astronomy, University of Iowa, Iowa City, Iowa 52242

Abstract

We evaluate the sensitivity of the Large Hadron Collider (LHC) to charged heavy vector boson production followed by their decays to $W^\pm Z^0$. We include the correlated decays of the gauge bosons to leptonic final states. With an integrated luminosity of 10^5 pb^{-1} , charged technirhos in the minimal $SU(N)_{TC}$ models for $N \geq 7$ yield signals with a significance larger than 5. In more general models, we explore the range of parameter space to which LHC experiments will be sensitive. Rapidity correlations exhibiting enhanced longitudinal gauge boson pair production are also shown.

I. INTRODUCTION

Anomalous weak diboson production at lepton [1] and hadron [2,3] colliders has been a topic of considerable interest because of its potential for exhibiting physics beyond the standard model at the TeV scale. In particular, non-standard physics may modify tri-boson couplings, yielding enhanced production of two electroweak gauge bosons. Modifications of the tri-boson couplings change the balance of purely longitudinally polarized final state bosons, purely transverse, and mixed polarization final states. Extracting vector boson polarizations at the Large Hadron Collider (LHC) will be a challenge. Our purpose here is to explore the enhancement of $W_L Z_L$ via their lepton decay modes in models with heavy vector boson intermediate states with couplings to longitudinal gauge bosons at the LHC.

Longitudinal weak boson enhancement is accomplished here with the introduction of a spin-one, isospin-one resonance (V) such as the technirho (ρ_T) that occurs in technicolor models [4]. Technicolor offers an alternative model to the standard model high energy behavior which is dominated by transverse gauge boson production. The enhancement of the cross section of longitudinal weak boson pairs comes because of s -channel production of technirho particles. We look at the charged technirho $\rho_T^\pm \rightarrow W^\pm Z$ and its generalization to $V^\pm \rightarrow W^\pm Z$ [5]. The advantage of this channel over the neutral channel: $V^0 \rightarrow W^+ W^-$ is that the neutral channel is plagued by the QCD background coming from $pp \rightarrow t\bar{t} \rightarrow W^+ W^- b\bar{b}$.

Compelling technicolor models which can account for mass generation in the fermion as well as the gauge boson sector are difficult to construct. We look at generic features of the coupling of a spin-one isospin-one vector boson which in a certain limit corresponds to the minimal technicolor model with one $SU(2)$ doublet of technifermions that transforms in the fundamental representation of the $SU(N)_{TC}$ gauge group [4]. In all of our calculations, we

assume that the direct coupling of V to fermions is negligible. Direct couplings to fermions would only improve our calculated signal rates.

Early analyses of vector boson production at high energy hadron colliders were done by Eichten, Hinchliffe, Lane and Quigg [6], Chanowitz and Gaillard [7] and Chivukula [8]. Later work on hadron collider production of V^\pm includes Refs. [9–13]. These analyses focused on vector boson distributions or a limited range of parameter space, including decays to leptons. Here, we include correlated gauge boson decays to leptons. We focus on the extent to which enhanced longitudinal boson production can be detected for a range of parameters which include the parameters of the minimal technicolor model. In addition to evaluating transverse mass distributions, we also exhibit rapidity correlations.

We find that the LHC has a limited range in parameter space for which heavy vector boson production will be clearly distinguishable from the standard model. Already by masses of 1.4 TeV, the minimal technicolor model is inaccessible with 10^5 pb^{-1} of integrated luminosity. We show that rapidity correlations will be a useful tool auxiliary to transverse mass distributions in the exploration of enhanced LL gauge boson pair production. In the next section we outline the parameters of the heavy vector boson models and the changes to the matrix elements required. In Section III we describe our results, followed by our conclusions in Section IV.

II. DI-BOSON PRODUCTION

A strongly-interacting symmetry breaking sector can be described in terms of an effective Lagrangian. The V particles are not fundamental particles, but composites of strongly interacting fermions. They should mix with photons, W 's and Z 's. Since we are focusing only on V^\pm , the mixing is with W^\pm . A generalization of minimal technicolor involving the heavy vector boson sector is described by the BESS (Breaking Electroweak Symmetry Strongly) model [5]. In this model, the V boson mass is

$$M_V^2 = \frac{1}{4}v^2 a g''^2 \quad (2.1)$$

in terms of $v = 246 \text{ GeV}$, a new coupling constant g'' and an arbitrary parameter a . Its width, in the $M_V \gg M_W, M_Z$ limit, is

$$\Gamma_V = \frac{a M_V^3}{192\pi v^2} . \quad (2.2)$$

Technicolor models follow from an effective Lagrangian which is assumed to scale directly from QCD dynamics involving the ρ . The Kawarabayshi-Suzuki-Fayyazudin-Riazuddin (KSFR) relations [14] between the mass and width of the vector boson should hold. They are satisfied when $a = 2$. Furthermore, the mass of the technirho is related to the N in $SU(N)_{TC}$ technicolor symmetry via

$$M_{\rho_T} = M_\rho \frac{F_{\pi_T}}{F_\pi} \left[\frac{3}{N} \right]^{1/2} \simeq 2 \text{ TeV} \left[\frac{3}{N} \right]^{1/2} \quad (2.3)$$

in the minimal one technifermion $SU(2)$ doublet version assumed here. In Eq. (2.3), $F_{\pi_T} = v$, $F_\pi = 93 \text{ MeV}$ is the pion decay constant and M_ρ is the ordinary ρ mass. The decay width

of ρ_T^\pm to the would-be goldstone boson pairs, namely, approximately the longitudinal boson pairs $W_L^\pm Z_L^0$, is $\Gamma(\rho_T^\pm \rightarrow W_L^\pm Z_L^0)$, which scales as $(3/N)^{3/2}$ in the large M_ρ limit. In these models, $\Gamma(\rho_T^\pm \rightarrow W_L^\pm Z_L^0)$ is the total decay width $\Gamma_{\rho_T^\pm}$. In the BESS model, the heavy vector boson decays only to $W_L^\pm Z_L^0$.

In our calculations below, we display results for minimal technicolor with several representative values of $M_{\rho_T^\pm}$ (several values of N). We evaluate technirho production for $N = 3 - 8$, corresponding to masses $M_{\rho^\pm} = 1.25 - 2.04$ TeV. In addition to considering $\Gamma(\rho_T^\pm \rightarrow W_L^\pm Z_L^0)$ given by Eq. (2.2) with $a = 2$, we consider a range of values for a in Eq. (2.2). The mass range evaluated here for the BESS generalization of technicolor ($a \neq 2$) is from 1–2.04 TeV. We generically represent the heavy vector resonance by V^\pm . We now turn to the matrix element squared.

As a consequence of the strongly interacting sector, the V^\pm can mix with W^\pm , and in s -channel interactions, enhance longitudinal gauge boson production as the parton invariant mass squared s approaches M_V^2 . In the process considered here ($pp \rightarrow WZ$), quarks, antiquarks and intermediate vector bosons are considered partons. Production of WZ can occur via $q\bar{q}'$ annihilation [15] and by vector boson scattering. We restrict our analysis to leading-order in QCD. Baur, Han and Ohnemus [3] have shown that the next-to-leading order standard model distributions for WZ production for quark-antiquark annihilation closely follow the leading order results in the $W^\pm Z^0 + 0$ jet case, where a jet requires $p_T(j) > 50$ GeV and $\eta(j) < 3$ [16]. For the subprocess $WZ \rightarrow WZ$ scattering, we use the effective-vector-boson approximation [17,18] (EVBA). Consequently, forward jet tagging, as discussed in for example Ref. [9], cannot be implemented. As a practical matter, the quark-antiquark annihilation process dominates.

For $q\bar{q}'$ annihilation, we have calculated the polarization cross sections $\sigma(q\bar{q}' \rightarrow W_i Z_j)$ for $i, j = T, L$ (transverse and longitudinal) polarizations directly using Form, [19] and using the program MadGraph [20]. The charged heavy vector boson modification of the cross section amounts to a substitution of the standard model matrix element squared for $q_i \bar{q}_j \rightarrow W_L^\pm Z_L$ by

$$|M(q_i \bar{q}_j \rightarrow W_L^\pm Z_L^0)|^2 \rightarrow |M(q_i \bar{q}_j \rightarrow W_L^\pm Z_L^0)|^2 \times \frac{a^2}{4} \frac{M_V^4}{(\hat{s} - M_V^2)^2 + M_V^2 \Gamma_V^2} \quad (2.4)$$

in terms of the mass M_V , width Γ_V , parameter a and parton center of mass energy squared \hat{s} . This is the conventional vector meson dominance (VDM) form accounting for $W^\pm - V^\pm$ mixing.

Vector boson scattering occurs in the standard model, however, it is not as large as $q\bar{q}'$ production of WZ at the LHC. The fusion of $W^\pm \gamma$ and $W^\pm Z^0$ intermediate states create $W^\pm Z^0$ final states. Using the improved vector boson approximation [18] which is a good representation of the perturbative process $q_i \bar{q}'_i \rightarrow q_f \bar{q}'_f (W^\pm \gamma, W^\pm Z^0) \rightarrow q_f \bar{q}'_f W^\pm Z^0$ [9], Kuss and Nuss [21] have shown that the vector boson scattering contribution to $\sigma(pp \rightarrow W^\pm Z^0)$ between WZ invariant masses of 0.5 TeV–2.0 TeV and pseudo-rapidity cuts of 2.5 is between 10–20% of the quark-antiquark annihilation contribution. The EVBA in the leading log approximation does well for the longitudinal scattering [21]. Consequently, we only consider vector boson scattering contributions involving longitudinal vector bosons in both the initial and final states in the case of enhanced couplings in the leading log approximation of the EVBA.

Using a generalized model of chiral coupling to vector mesons, the longitudinal matrix element is [10]

$$M(W_L^\pm Z_L^0 \rightarrow W_L^\pm Z_L^0) = \left(1 - \frac{3}{4}a\right) \left(\frac{\hat{t}}{v^2}\right) + \frac{a M_V^2}{4 v^2} \left(\frac{\hat{u} - \hat{t}}{\hat{s} - M_V^2 + iM_V \Gamma_V} + \frac{\hat{s} - \hat{t}}{\hat{u} - M_V^2}\right), \quad (2.5)$$

in terms of Mandelstam variables \hat{s} , \hat{t} and \hat{u} , which are combinations of W and Z momenta. The longitudinal matrix element potentially has unitarity problems associated with the behavior at large \hat{s} . In particular, the isospin-two, spin-zero partial wave amplitude has no resonant structure. Following Refs. [9,10], by setting the real part of the two body partial wave amplitude to less than 1/2 for energies up to $\sqrt{\hat{s}} = 1.5M_V$, the parameter a is constrained to be in the range

$$\text{Max}\left(3 - 4.1\left(\frac{\text{TeV}}{M_V}\right)^2, 0\right) \leq a \leq 3 + 4.1\left(\frac{\text{TeV}}{M_V}\right)^2. \quad (2.6)$$

We demonstrate below that the LHC will be sensitive to a range of a consistent with the unitarity limit.

The parton differential cross section in the parton center of mass frame is

$$\frac{d\hat{\sigma}}{d\cos\theta} = \frac{1}{32\pi\hat{s}} |M|^2. \quad (2.7)$$

The hadron-hadron cross section is

$$\sigma = \sum_{ij} \int dx_1 dx_2 d\cos\theta f_{i/p}(x_1, Q^2) f_{j/p}(x_2, Q^2) \frac{d\hat{\sigma}}{d\cos\theta} \quad (2.8)$$

where i, j include sums over quark flavors and the $W_L Z_L$ initial states. We take $Q = \sqrt{\hat{s}}$ in the MRSA parton distribution functions [22]. The calculations are done at $\sqrt{S} = 14$ TeV in proton-proton collisions.

The decay modes of interest are purely leptonic. We count a single charged lepton decay mode for each boson decay. In dealing with $Z \rightarrow l^+ l^-$, we assume that the Z four-momentum is well reconstructed. Since we have evaluated each polarization matrix element separately for $pp \rightarrow WZ$, we include the polarized $W \rightarrow l\nu$ decay matrix elements. In all cases, we sum over both charges of the W boson.

III. RESULTS

We begin by showing in Figs. 1 and 2 the transverse mass distributions including technirho production ($a = 2$) for $pp \rightarrow W^\pm Z^0 \rightarrow l_1 \nu_1 l_2 \bar{l}_2$, assuming $N = 8$ (Fig. 1) and $N = 3$ (Fig. 2). Only one channel for the W boson decay and the Z boson decay is included. The transverse mass is defined by

$$m_T^2 = [(\vec{p}_T(Z) + m_Z^2)^{1/2} + ((\vec{p}_T(l_1) + \vec{p}_T)^2 + m_W^2)^{1/2}]^2 - (\vec{p}_T(Z) + \vec{p}_T(l_1) + \vec{p}_T)^2. \quad (3.1)$$

The neutrino transverse momentum is indicated by \vec{p}_T . The dominant background source to heavy boson production followed by decay to $W^\pm Z^0$ is the transverse boson pair production.

The background is reduced by requiring the Z and the charged lepton from W decay to lie in the central region of the detector. In all of the results shown, we have imposed the following rapidity cuts:

$$\begin{aligned} |y_Z| &< 2.5, \\ |y_{l_1}| &< 2.5, \end{aligned} \tag{3.2}$$

where the lepton l_1 comes from W^\pm decay.

Transverse mass plots have the separate contributions by transverse-transverse (TT) WZ bosons indicated by the solid line, longitudinal-longitudinal (LL) by dashed lines and mixed (TL+LT) contributions shown by dot-dashed lines. The polarizations are defined in the parton center-of-mass frame. The contribution labeled LL-VDM comes from $q\bar{q}'$ annihilation to a heavy technirho, while the LL-VBS contribution comes from vector boson scattering as in Eq. (2.5). The dashed line labeled LL is the standard model LL result. The heavy solid line is the sum of the TT, TL+LT and nonstandard LL contributions.

As can be seen from Fig. 1, low mass ($N = 8$, $M_\rho = 1.25$ TeV) technirho production will be visible as a peak in the transverse mass distribution. Vector boson scattering has a small contribution at $\sqrt{S} = 14$ TeV. For $M_\rho = 2.04$ TeV ($N = 3$), the transverse mass peak is less well defined, as the technirho width is 466 GeV in the minimal technicolor model. Statistics will play an important role for the higher mass range.

In Table I, we show the cross section for $pp \rightarrow W^\pm Z^0 \rightarrow l_1 \nu_1 l_2 \bar{l}_2$ at the LHC for $m_T \geq 0.5$ TeV, in units of 10^{-4} pb, including technicolor $N = 8$ (TC8), $N = 4$ (TC4) and $N = 3$ (TC3) for representative nonstandard model values. Both quark-antiquark annihilation and vector boson scattering are included in the nonstandard model results. For the proposed integrated luminosity of the LHC, $\int dt\mathcal{L} = 10^5$ pb $^{-1}$, the number of events that come from diagrams with a technirho is on the order of $\sim 20 - 80$ events, depending on the value of the mass. The standard model prediction for the same integrated luminosity and minimum transverse mass is ~ 70 events.

Table II shows the minimum luminosity required to detect the technirho with a significance,

$$\text{Significance} = \frac{S}{\sqrt{S+B}} \geq 5. \tag{3.3}$$

We define the signal to be the difference between the LL distributions with and without nonstandard model modifications. The background is the sum of all standard model contributions to the distribution. We have chosen transverse mass cuts to maximize the significance, limited by our bin size of 25 GeV. The minimum transverse mass which maximizes the significance varies from 725 GeV ($N = 8$) to 1075 GeV ($N = 3$). The $N = 7$ and $N = 8$ technicolor models are accessible to the LHC in this single channel final state, given an integrated luminosity $\int dt\mathcal{L} = 10^5$ pb $^{-1}$ and the requirement that the significance is greater than 5.

An interesting distinction between standard model and technirho enhanced LL production is seen in WZ rapidity correlations. Baur, Han and Ohnemus [23] have shown that there are zeros in leading order matrix elements contributing to the TT cross section. Non-standard LL enhancement fills in the zeros. Next-to-leading order contributions also tend to fill in the zeros, but by imposing a zero-jet cut, the NLO effects can be largely ignored

[3], as mentioned above. Since the W decays to a charged lepton and neutrino, some of the correlation is washed out, nevertheless, there is a pronounced difference in the shape of the distribution in

$$\Delta y_{Zl} \equiv y_Z - y_{l_1} . \quad (3.4)$$

Figs. 3 and 4 show the cross section $\Delta\sigma$ in each bin in Δy_{Zl} of size 0.2 for $N = 8$ and $N = 3$, respectively. The solid line shows the standard model result, while the dashed line shows the sum of the TT, TL+LT and nonstandard LL. The rapidity cuts in Eq. (3.2) are imposed, and the transverse mass is restricted to yield the highest significance. For Fig. 3, $725 \text{ GeV} \leq m_T \leq 1600 \text{ GeV}$, while for Fig. 4, $1075 \text{ GeV} \leq m_T \leq 2400 \text{ GeV}$.

The shapes of the Δy_{Zl} distributions for the standard model and technirho are dramatically different. In Fig. 3, the nonstandard curve is peaked at $\Delta y_{Zl} = 0$ and changes by a factor of ~ 5 in the range from $|\Delta y_{Zl}| = 2$ to $|\Delta y_{Zl}| = 0$. The standard curve changes by less than a factor of 1.25 and exhibits a slight dip at $\Delta y_{Zl} = 0$. The corresponding change in Fig. 4 for the non-standard model is more than a factor of 3 while the standard model changes by less than a factor of 1.5.

In the more general context of the BESS model, the mass and width are related by the parameter a . In addition, with increasing a , heavy vector boson production is enhanced. For large enough a , even a heavy vector boson of mass 2 TeV is detectable at the LHC with 10^5 pb^{-1} of integrated luminosity. In Table III we show the minimum a (a_{min}) that gives a significance $S/\sqrt{S+B} \geq 5$. We have applied the rapidity cuts from Eq. (3.2). The transverse mass cuts are fixed to maximize the significance of the signal, however, not set lower than 500 GeV. The resulting values of a_{min} range from 0.42-3.9 for $m_V = 1.00 - 2.04$ TeV. These values of a_{min} lie within the limits required by partial wave unitarity in Eq. (2.6).

Figs. 5 and 6 show the transverse mass distributions for $m_V = 1.00$ TeV, $a = 0.42$ and $m_V = 2.04$ TeV, $a = 3.9$, respectively. Figs. 7 and 8 show the corresponding $\Delta\sigma$ versus Δy_{Zl} distributions. The feature of the narrow peak in the transverse mass distribution for the 1 TeV heavy vector boson will make the signal stand out. The resonant peak for $m_V = 2.04$ TeV is much less distinct, and the Δy_{Zl} distribution provides auxiliary evidence of enhanced longitudinal gauge boson production.

IV. CONCLUSIONS

Direct measurements of $pp \rightarrow W^\pm Z^0 \rightarrow l_1 \nu_1 l_2 \bar{l}_2$ at the LHC will constrain models with charged vector bosons coupling to longitudinal W 's and Z 's. In the case of minimal technicolor with one SU(2) doublet of technifermions, $N \geq 7$ in $SU(N)_{TC}$ for a significance equal to 5 or more given 10^5 pb^{-1} integrated luminosity. If one considers the more general BESS model, an additional parameter a is introduced. The minimum a ranges from 0.42–3.9 for $M_V = 1 - 2.04$ TeV if one requires a significance of 5. Rapidity correlations demonstrate enhanced longitudinal gauge boson production and may be an important tool in identifying the nature of nonstandard model enhancements of weak gauge boson pair production.

Constraints on BESS and technicolor parameters from precision electroweak measurements have been evaluated by Casalbuoni et al. [24] and updated by Dominici in Ref. [25].

Heavy vector bosons contribute to the oblique parameter ϵ_3 through radiative corrections to the vector and axial vector weak couplings. Analyses of high energy experimental data [26] yield $\epsilon_3^{exp} = (4.1 \pm 1.4) \cdot 10^{-3}$. Standard model radiative corrections, setting $m_H = 1$ TeV, give $\epsilon_3^{th} = (6.6 \pm 0.1) \cdot 10^{-3}$. In the case in which there is not a fundamental Higgs boson, the radiative contribution to ϵ_3 has the same form as the Higgs contribution, and is approximately equal if one takes the cutoff at $\Lambda = 1$ TeV [24]. Taking the difference between the two values, nonstandard contributions to ϵ_3 which come in at the tree level, as is the case here, are limited to

$$\epsilon_3 < 1.7 \cdot 10^{-3} \quad (4.5 \cdot 10^{-3}) \quad (4.1)$$

at the 3σ (5σ) level.

The standard technicolor model has contributions to ϵ_3 from both heavy vector and heavy axial vector bosons. The axial vector contributions come in with opposite sign in a prescribed ratio. The net result is that $M_{\rho_T} > 2.38$ TeV (3σ) and $M_{\rho_T} > 1.46$ TeV (5σ), requiring the N of $SU(N)$ to be $N < 2.1$ or $N < 5.6$, respectively.

In the case of the more general BESS model, there are no set relations between vector and axial vector masses, so the limits are weaker. In the case of degenerate heavy vector and axial vector bosons [25], $\epsilon_3 \sim aM_W^4/M_V^4$. The limits in the degenerate case are not especially relevant to the calculation here because we have not included a degenerate axial vector boson contribution to the signal. In the case where the heavy axial vector boson contribution to ϵ_3 can be ignored, $a < 0.27(M_V/\text{TeV})^2$ for the 3σ case, and $a < 0.71(M_V/\text{TeV})^2$ for 5σ case.

The indirect limits on standard technicolor and the BESS model in the absence of heavy axial vector boson corrections are in general stronger than the potential LHC limits, but rely on the approximation of the radiative corrections. The LHC experiments will provide important direct constraints on the existence of charged heavy vector bosons.

ACKNOWLEDGMENTS

Work supported in part by National Science Foundation Grant No. PHY-9507688 and PHY-9802403.

REFERENCES

- [1] See, for example, F. M. Renard, S. Spagnolo, C. Verzegnassi, Phys. Lett. B **409**, 398 (1997); M. Diehl and O. Nachtmann, Eur. Phys. J. C **1**, 177 (1998); A. Blondel, F. M. Renard and C. Verzegnassi, Phys. Rev. D **54**, 5567 (1996); and references therein.
- [2] See, for example, D. Zeppenfeld and S. Willenbrock, Phys. Rev. D **37**, 1775 (1988); M. Kuroda, J. Maalampi, K. H. Schwarzer and D. Schildknecht, Nucl. Phys. **B284**, 271 (1987); S.-C. Lee and W.-C. Su, Phys. Lett. B **212**, 113 (1988); K. Hagiwara, J. Woodside and D. Zeppenfeld, Phys. Rev. D **41**, 2113 (1990); J. Bagger, S. Dawson and G. Valencia, Nucl. Phys. **B399**, 364 (1993); K. R. Barger and M. H. Reno, Phys. Rev. D **51**, 90 (1995); E. Nuss, Z. Phys. C **76**, 701 (1997).
- [3] U. Baur, T. Han and J. Ohnemus, Phys. Rev. D **51**, 3381 (1995).
- [4] S. Weinberg, Phys. Rev. D **13**, 974 (1976); Phys. Rev. D **19**, 1277 (1979); L. Susskind, Phys. Rev. D **20**, 2619 (1979); S. Dimpoulos, Nucl. Phys. **B168** (1980) 69; S. Dimpoulos, S. Raby and G. Kane, Nucl. Phys. **B182** (1981) 77.
- [5] R. Casalbuoni, S. DeCurtis, D. Dominici and R. Gatto, Phys. Lett. B **155**, 95 (1985); Nucl. Phys. **B282**, 235 (1987).
- [6] E. Eichten, I. Hinchliffe, K. Lane and C. Quigg, Rev. Mod. Phys. **56**, 579 (1984); *errata* *ibid* **58** (1986) 1065.
- [7] M. S. Chanowitz and M. K. Gaillard, Nucl. Phys. **B261**, 379 (1985).
- [8] R. S. Chivukula, "Technivector meson production at the SSC," in *Proc. of the Johns Hopkins Workshop on Current Problems in Particle Theory 12: TeV Physics*, ed. G. Domokos and S. Kovesi-Domokos, (World Scientific, New Jersey, 1988).
- [9] J. Bagger et al., Phys. Rev. D **49**, 1246 (1994); J. Bagger et al., Phys. Rev. D **52**, 3878 (1995).
- [10] J. Bagger, T. Han and R. Rosenfeld, in *Research Directions for the Decade*, Proceedings of the Summer Study, Snowmass, Colorado, 1990, edited by E. Berger (World Scientific, Singapore, 1992) p. 208.
- [11] R. Casalbuoni et al., Phys. Lett. B **249**, 130 (1990).
- [12] A. Dobado, M. Herrero and J. Terron, Z. Phys. C **50**, 205 (1991); Z. Phys. C **50**, 465 (1991).
- [13] M. Chanowitz and W. Kilgore, Phys. Lett. B **322**, 147 (1994).
- [14] K. Kawarabayshi and M. Suzuki, Phys. Rev. Lett. **16**, 255 (1966); Riazuddin and Fayyazudin, Phys. Rev. **147**, 1071 (1966).
- [15] R. W. Brown and K. O. Mikaelian, Phys. Rev. D **19**, 922 (1979); R. W. Brown, D. Sahdev and K. O. Mikaelian, Phys. Rev. D **20**, 1164 (1979).
- [16] NLO corrections have also be evaluated by S. Frixione, P. Nason and G. Ridolfi, Nucl. Phys. **B383**, 3 (1992).
- [17] S. Dawson, Nucl. Phys. **B249**, 42 (1985); G. L. Kane, W. W. Repko and W. B. Rolnick, Phys. Lett. B **148**, 367 (1985); M. S. Chanowitz and M. K. Gaillard, Phys. Lett. B **142**, 85 (1984).
- [18] I. Kuss, Phys. Rev. D **55** (1997) 7165.
- [19] J. A. M. Vermaseren, KEK-TH-326, March 1992.
- [20] T. Stelzer and W. F. Long, Comp. Phys. Commun. **81** (1994) 357.
- [21] I. Kuss and E. Nuss, Eur. Phys. J. C **4**: 641, 1998.
- [22] A. D. Martin, R. G. Roberts, W. J. Stirling, Phys. Rev. D **50** (1994) 6734.

- [23] U. Baur, T. Han and J. Ohnemus, Phys. Rev. Lett. **72**, 3941 (1994).
- [24] R. Casalbuoni, S. DeCurtis, D. Dominici, F. Feruglio and R. Gatto, Phys. Lett. B **269**, 361 (1991).
- [25] D. Dominici, Riv. Nuo. Cim. **20**, 1 (1997).
- [26] G. Altarelli, R. Barbieri and F. Caravaglios, Int. J. Mod. Phys. A **13** (1998) 1031.

TABLES

TABLE I. Cross section for $pp \rightarrow W^\pm Z^0 \rightarrow l_1 \nu_1 l_2 \bar{l}_2$ at the LHC for $m_T \geq 0.5$ TeV, in units of 10^{-4} pb. Rapidity cuts $|y_Z|, |y_{l_1}| < 2.5$ were applied.

Polarization	σ
TT	4.62
TL	0.23
LT	0.25
LL	1.66
LL-TC8	8.19
LL-TC4	2.98
LL-TC3	2.35

TABLE II. Minimum luminosity for the detection of charged technirhos ($a = 2$) at the LHC for a calculated significance greater than 5, assuming one channel for each boson decay.

M_V [TeV]	\mathcal{L}_{\min} [10^5 pb $^{-1}$]
1.25 ($N = 8$)	0.6
1.34 ($N = 7$)	0.9
1.44 ($N = 6$)	1.5
1.58 ($N = 5$)	2.3
1.76 ($N = 4$)	5.9
2.04 ($N = 3$)	17.4

TABLE III. Limits on a for $pp \rightarrow W^\pm Z^0 \rightarrow l_1^\pm \nu_1 l_2^\pm \bar{l}_2^\mp$ at the LHC with 10^5 pb $^{-1}$ of luminosity. We have imposed rapidity cuts $|y_Z|, |y_{l_1}| < 2.5$. Transverse mass cuts are fixed to maximize the significance of the signal.

M_V [TeV]	a_{\min}
1.00	0.42
1.25	1.4
1.76	3.4
2.04	3.9

FIGURES

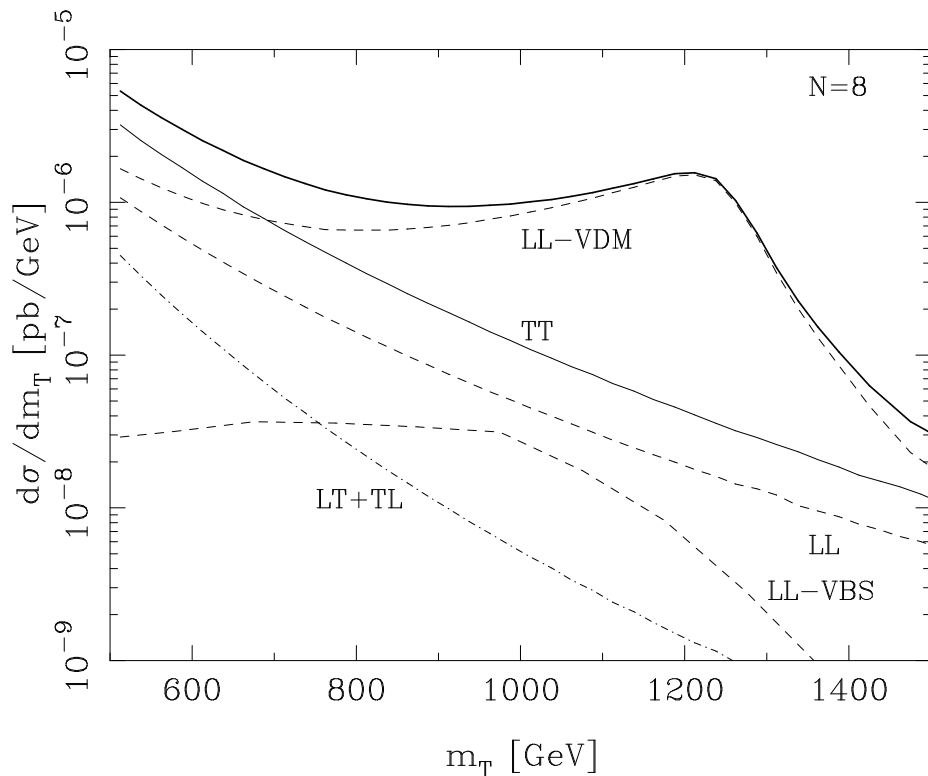


FIG. 1. Differential cross section, including technirho ($a=2$) contributions, as a function of m_T for $pp \rightarrow W^\pm Z^0 \rightarrow l_1 \nu_1 l_2^+ l_2^-$ at the LHC. The solid line is the sum of the transverse boson final states (TT), the dashed line labeled LL is the standard model longitudinal pair distribution and the mixed transverse-longitudinal pair (TL+LT) is shown by the dot-dashed line. The technicolor contribution via $q\bar{q}'$ annihilation is shown by the dashed line labeled by LL-VDM, while the vector boson scattering contribution is labeled LL-VBS. The technirho contribution assumes $N = 8$ ($M_{\rho_T} = 1.25$ TeV).

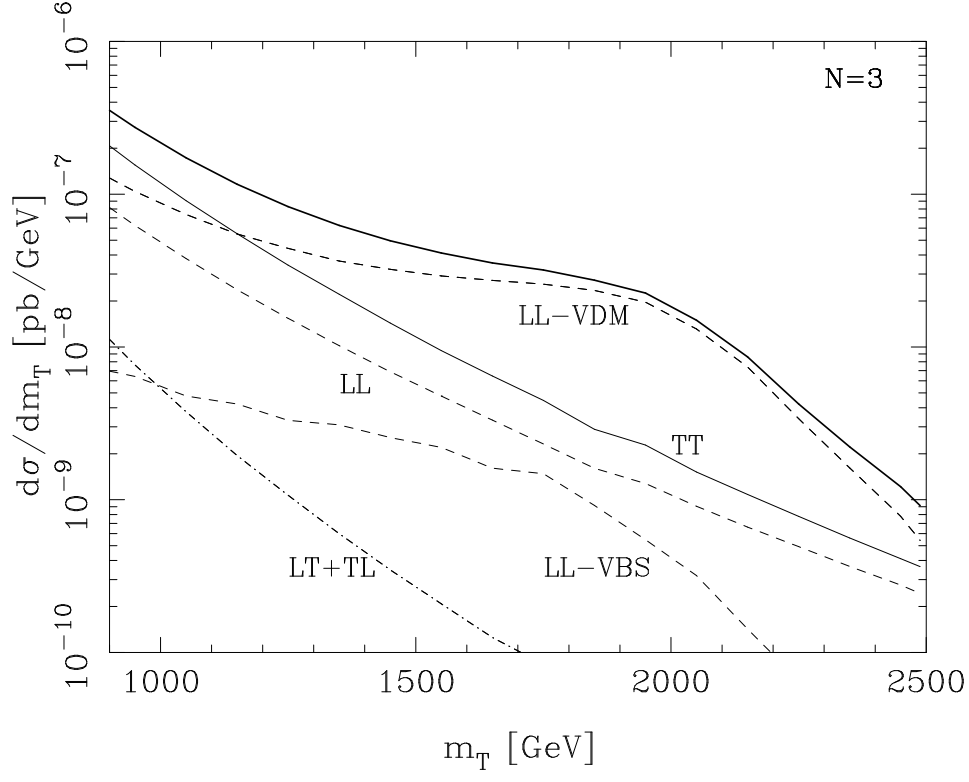


FIG. 2. As in Fig. 1, here with $N = 3$ ($M_{\rho_T} = 2.04$ TeV).

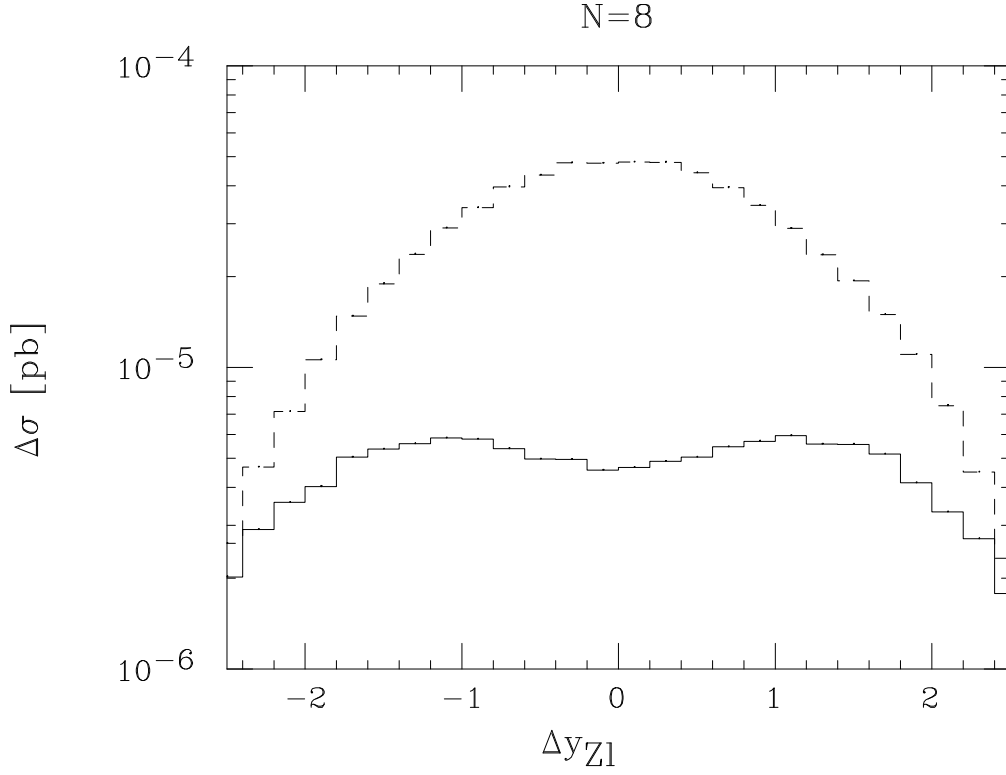


FIG. 3. Cross section, per bin of 0.2 in rapidity, as a function of Δy_{Z1} for $725 \text{ GeV} \leq m_T \leq 1600 \text{ GeV}$. The solid histogram shows the standard model result. The dashed histogram shows the signal plus background for $N = 8$ minimal technicolor.

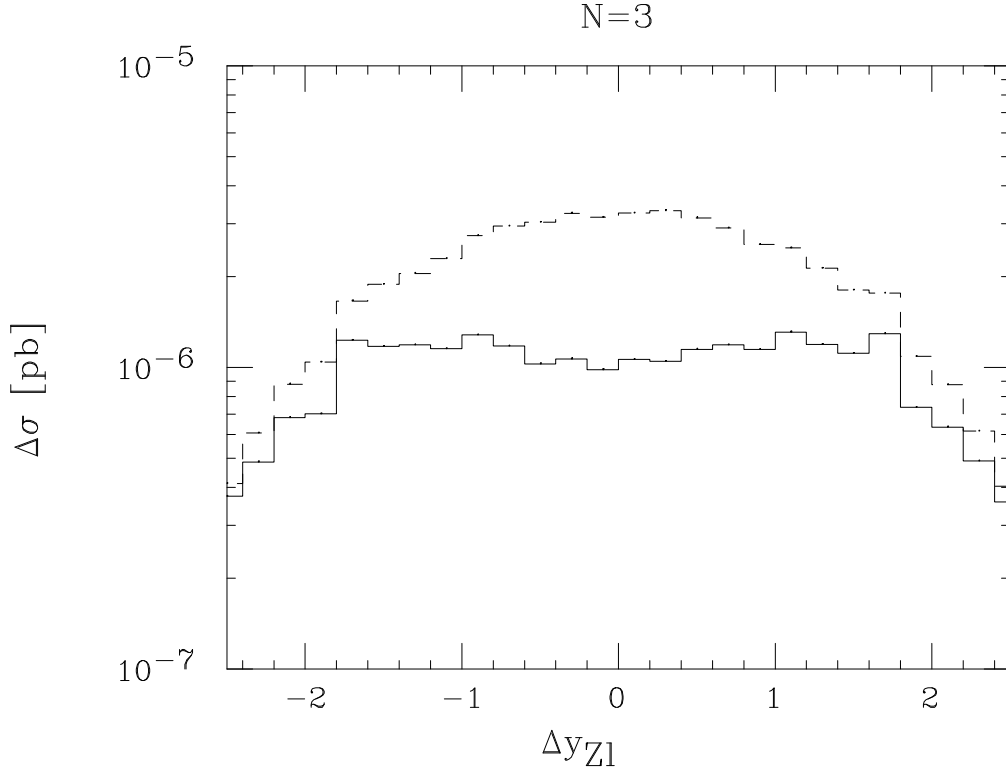


FIG. 4. Cross section, per bin of 0.2 in rapidity, as a function of Δy_{Z1} for $1075 \text{ GeV} \leq m_T \leq 2400 \text{ GeV}$. The solid histogram shows the standard model result. The dashed histogram shows the signal plus background for $N = 3$ minimal technicolor.

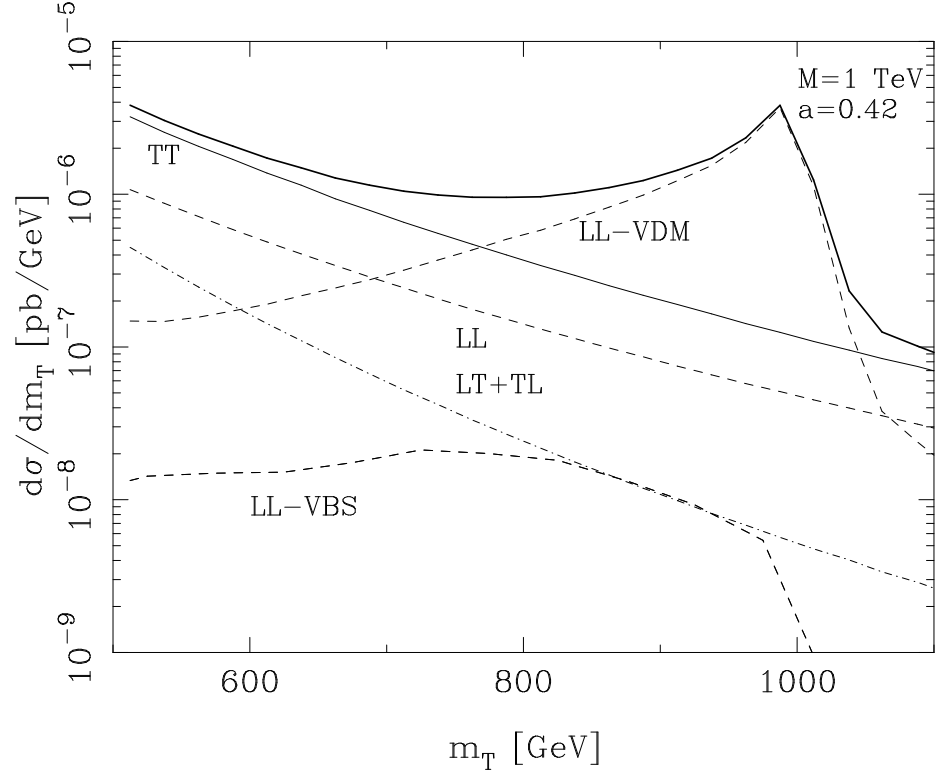


FIG. 5. Differential cross section as a function of m_T for $M_V = 1.00$ TeV and $a = 0.42$. The curves are labeled as in Figure 1.

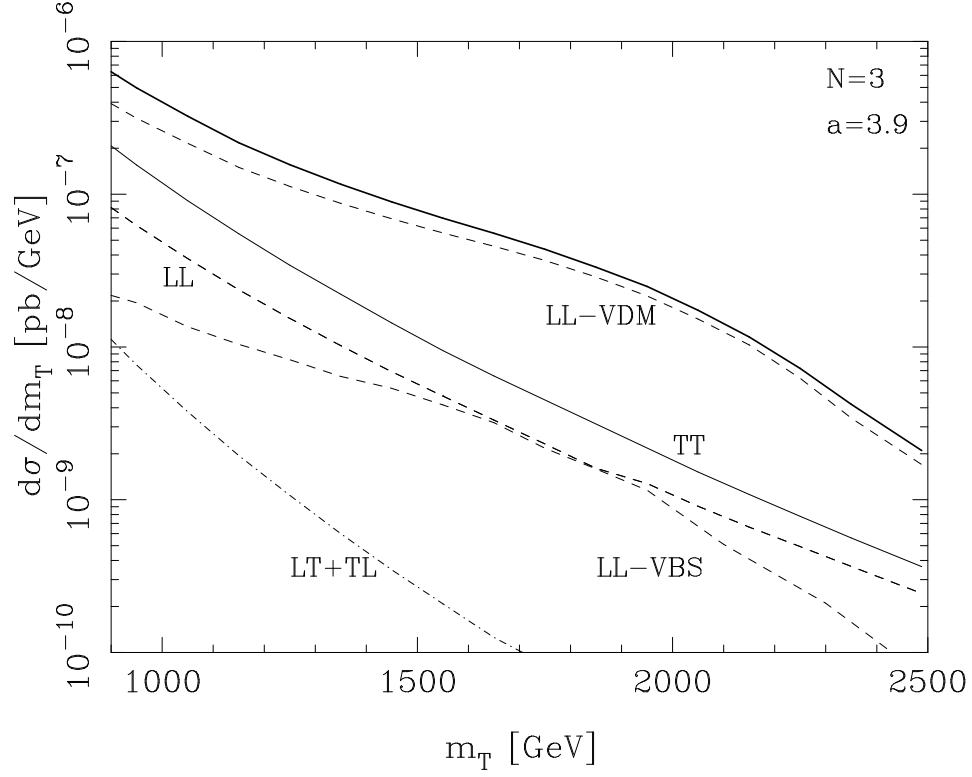


FIG. 6. Differential cross section as a function of m_T for $M_V = 2.04$ TeV and $a = 3.9$. The curves are labeled as in Figure 1.

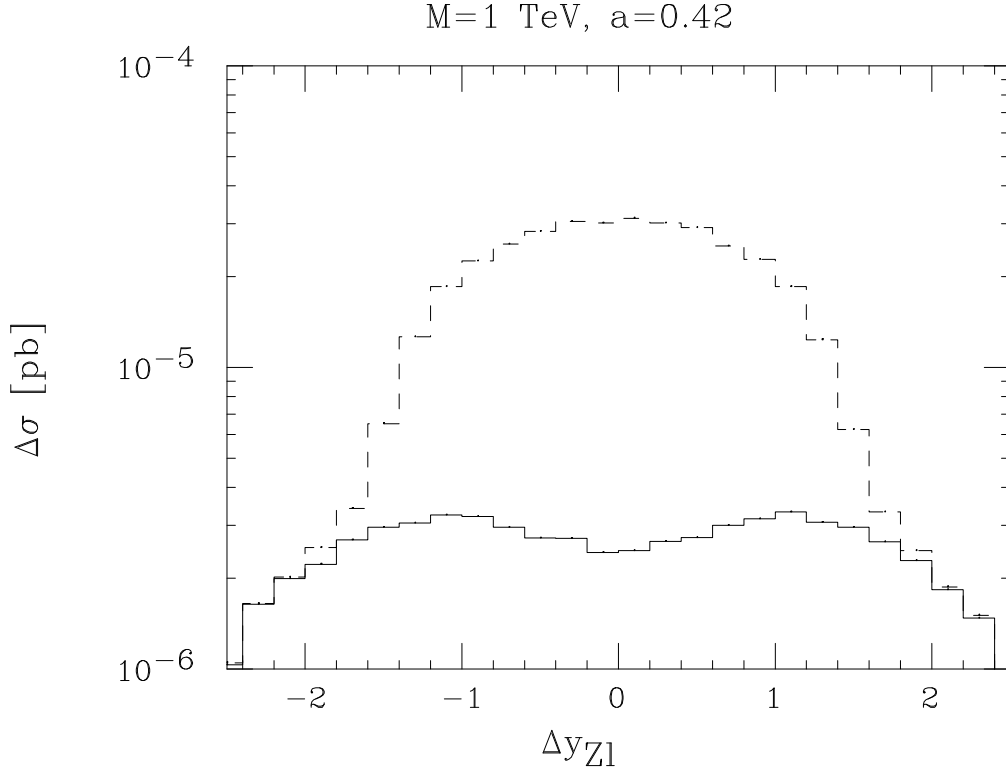


FIG. 7. Cross section, per bin of 0.2 in rapidity, as a function of Δy_{Z1} for $M = 1.00$ TeV, $a = 0.42$ and $800 \text{ GeV} \leq m_T \leq 1050 \text{ GeV}$. The solid histogram shows the standard model result. The dashed histogram shows the signal plus background for $N = 8$ minimal technicolor.

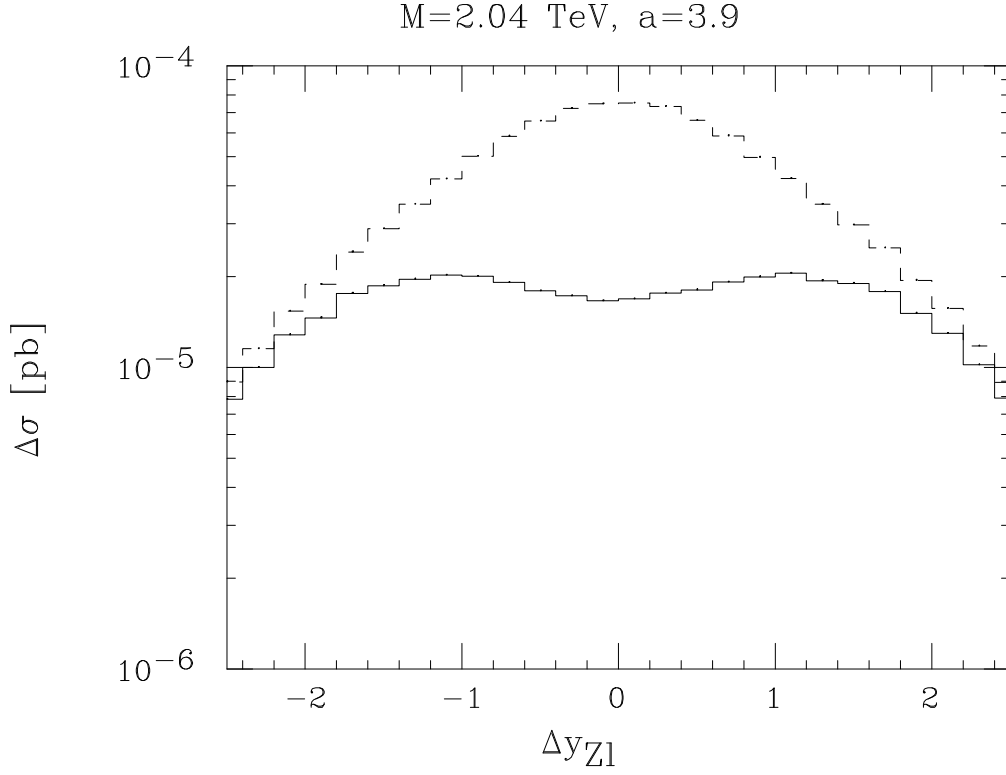


FIG. 8. Cross section, per bin of 0.2 in rapidity, as a function of Δy_{Z1} for $M = 2.04$ TeV, $a = 3.9$ and $500 \text{ GeV} \leq m_T \leq 2500 \text{ GeV}$. The solid histogram shows the standard model result. The dashed histogram shows the signal plus background for $N = 8$ minimal technicolor.